Materials Research
Express

INCLUSIVE PUBLISHING TRUSTED SCIENCE
PURPOSE-LED PUBLISHING™

PAPER • OPEN ACCESS

Cleaved surfaces and homoepitaxial growth of InBi(001)

To cite this article: Thomas J Rehaag *et al* 2025 *Mater. Res. Express* **12** 096506

View the article online for updates and enhancements.

You may also like

- Robust topological insulating property in C_2X-functionalized III-V monolayers
Xianghong Xue, Zhihua Lin, Rui Gao et al.

- Unveiling the Sodium/Potassium Storage Mechanisms of Nanoporous Indium-Bismuth Anode Using Operando X-ray Diffraction
Zhiyuan Guo, Jingyu Qin, Bin Yu et al.

- Raman scattering studies of dilute $InP_{1-x}Bi_x$ alloys reveal unusually strong oscillator strength for Bi-induced modes
Wenwu Pan, J A Steele, Peng Wang et al.

This content was downloaded from IP address 137.205.72.18 on 02/01/2026 at 19:31

IOP Publishing *Mater. Res. Express* **12** (2025) 096506 https://doi.org/10.1088/2053-1591/adfc2d

Materials Research Express

OPEN ACCESS

RECEIVED
3 April 2025

REVISED
3 July 2025

ACCEPTED FOR PUBLICATION
15 August 2025

PUBLISHED
19 September 2025

Original content from this work may be used under the terms of the Creative Commons Attribution 4.0 licence.

Any further distribution of this work must maintain attribution to the author(s) and the title of the work, journal citation and DOI.

PAPER

Cleaved surfaces and homoepitaxial growth of InBi(001)

Thomas J Rehaag[1], **Daniel A Mayoh**[1], **Tomáš Bárta**[1,2], **Freya Slaney-Parker**[1], **Ibrahim Elhoussieny**[1,3], **Ján Minár**[2] **and Gavin R Bell**[1,*]

[1] Department of Physics, University of Warwick, Coventry CV 4 7AL, United Kingdom
[2] Department of Physics, University of West Bohemia, Plzen 30614, Czech Republic
[3] Department of Physics, Ain Shams University, Cairo 11566, Egypt
[*] Author to whom any correspondence should be addressed.

E-mail: gavin.bell@warwick.ac.uk

Keywords: InBi, topological semimetal, surface, homoepitaxy

Supplementary material for this article is available online

Abstract

InBi is a semimetal with topologically non-trivial electronic surface states, which is also chemically and structurally compatible with conventional III-V semiconductors. Single crystal InBi has been grown and its (001) cleave surfaces studied. They do not conform to the single Bi-Bi cleave plane previously assumed in band structure studies of the material but instead expose both In- and Bi-terminated surface regions. Crystals cleaved in ultra-high vacuum have been used as substrates for ultra-low temperature homoepitaxy via periodic supply epitaxy (PSE) with alternate Bi and In fluxes. Homoepitaxial growth of good quality InBi was not achieved under these conditions. The 3D and 2D surface structures produced by PSE were studied by reflection high energy electron diffraction and atomic force microscopy. By studying InBi homoepitaxy for the first time, this work highlights the challenge of growing high quality InBi epilayers beyond the ultra-thin heteroepitaxial layers recently demonstrated [Molecules 2024, 29(12), 2825].

1. Introduction

Topological insulators and semimetals can support electronic surface and interface states with remarkable properties such as Dirac-like dispersion, suppressed backscattering, and spin-momentum locking [1]. They have been the subject of strong interest in the condensed matter physics community [2, 3] and numerous potential applications have been proposed [4–6] including low power memory / processing [7, 8] and thermoelectric energy harvesting [9–11]. However, serious challenges in material synthesis, stability and compatibility remain in developing practical technologies with such materials [12–14]. It has long been recognized that thin-film materials compatibility is very important [15–18] and monolithic integration with an existing well-established electronic materials system is a major advantage. One such system is the III-V semiconductors, for which epitaxial growth of highly controlled heterostructures is routine, for example by molecular beam epitaxy (MBE). Epitaxial topological materials can have properties adjusted by film thickness, for example via quantum confinement of bulk states and tunable coupling of upper and lower interface states [19].

Among the III-V compounds only InBi is not a semiconductor (i.e. does not show a nonzero band gap), and recently it has been shown to support topologically nontrivial states [20]. InBi is chemically compatible with other III-V materials. In particular, both In and Bi are routinely used in III-V MBE, and so many existing growth reactors could support InBi growth without modification. Structural compatibility between tetragonal InBi and cubic III-V materials is also good, with two possible epitaxial relationships found on InSb(001) [21] which may facilitate monolithic integration. However, InBi growth by MBE is difficult, partly because its melting point is only 109°C [22], which is much lower than typical substrate temperatures used for III-V MBE. Several groups have attempted heteroepitaxial growth of InBi from ultra-thin 2D layers to thick films [23–25]. Reflection high energy electron diffraction (RHEED) patterns disappear almost instantaneously on InBi deposition by MBE and

© 2025 The Author(s). Published by IOP Publishing Ltd

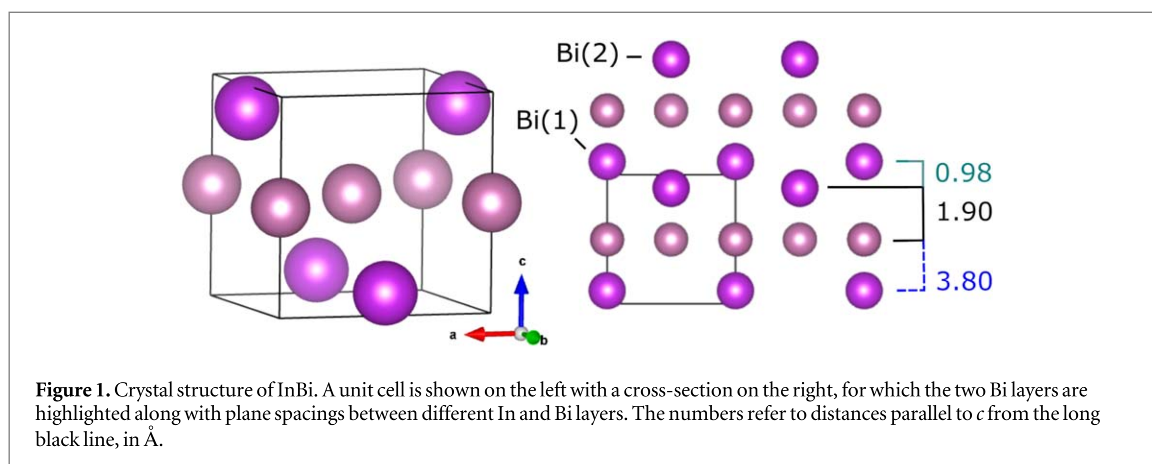

Figure 1. Crystal structure of InBi. A unit cell is shown on the left with a cross-section on the right, for which the two Bi layers are highlighted along with plane spacings between different In and Bi layers. The numbers refer to distances parallel to *c* from the long black line, in Å.

surfaces are prone to droplet formation [23]. Thicker layer growth of InBi can be achieved by an overpressure of Bi, increasing the melting point and preventing droplet formation, but also increasing the density of pure Bi phase within the film [24].

Interestingly, lattice mismatch did not have a significant effect on the quality of InBi MBE-grown films [23]. Growth on (100) yttria stabilized zirconium (effective mismatch only 3%) reportedly yielded similar film quality to growth on GaAs (effective mismatch 13%) [23]. This may relate to the natural cleavage of InBi, in its (001) plane, which corresponds to weaker chemical bonding both within the material and across its interface with the substrate, allowing large mismatches to be accommodated in a manner similar to van der Waals epitaxy. Ultra-thin epitaxial InBi with higher crystal quality has recently been grown on InSb(001) substrates by low temperature MBE and periodic supply epitaxy (PSE) [21]. Depending on the growth conditions, different in-plane epitaxial orientations of the InBi(001) layers arose, highlighting the weaker film-substrate interaction. It must also be noted that InBi does not adopt either the B3 zincblende or B4 wurtzite structures of the other III-Vs. Instead it is tetragonal, space group P4/nmm, with $a = b = 5.01$ Å and $c = 4.78$ Å [20, 26].

Recently, InBi(001) has been formed epitaxially on InAs(111), in domain structures alongside Bi(111) [27]. The band structure was investigated by angle resolved photoemission spectroscopy (ARPES) and topological surface states found near the $\overline{M}$ high symmetry point of InBi. These were associated with a predominantly Bi bilayer-terminated (001) surface as opposed to the Bi monolayer (ML) terminated surface previously assumed [20]. The crystal structure and (001) surface terminations of InBi are shown in figure 1. The Bi ML termination is generated by cleaving the crystal between the Bi(1) and Bi(2) layers, resulting in a step height of $3.80 + 0.98 = 4.78$ Å. However, an average step height smaller by a factor of 2 was observed by scanning tunneling microscopy (STM) for InBi(001) on InAs, together with distinctly different atomic-scale contrast on alternating terraces [27]. This is explained by termination with *both* In and Bi bulk layers. Assuming some relaxation within the Bi(1) + Bi(2) bilayer, this gives step heights of 2.2 to 2.6 Å. Co-existing V-rich and III-rich surface domains can only be observed on III-V semiconductors in non-equilibrium situations, such as being quenched in during 3D island nucleation [28] or during a reconstruction transition [29], or in the presence of liquid metal droplets which locally alter the chemical potential [30, 31]. InBi appears to be an exception to this rule.

The results demonstrated for InBi on GaAs, InSb and InAs suggest that integration of InBi with the family of III-V semiconductors is a realistic goal. However, more needs to be understood about its epitaxial behavior and about the growth of III-Vs on InBi surfaces. Bulk single crystals of InBi provide a useful tool to address both questions. In this paper we describe growth of bulk InBi crystals and homoepitaxial growth of InBi on their cleaved surfaces by PSE. This allows us to test homoepitaxial growth of InBi by MBE / PSE, which has not previously been attempted. While we do not study the heteroepitaxial overgrowth of III-V semiconductor materials on InBi in this work, in order to understand and optimize this growth the nature of the cleaved surface of InBi(001) will need to be understood. We therefore study this cleave surface in the present paper and show that the cleaved crystal terminates with both In and Bi bulk layers. This result was previously observed for epitaxial material [27] and has implications for both heteroepitaxial integration and for surface-sensitive ARPES studies of the topological electronic surface states of cleaved InBi.

2. Experimental section

Single crystals of InBi were grown by the modified Bridgman technique [32]. A mixture of In (99.99999%, Wafer Technology Ltd.) and Bi (99.9999%, American Elements) with a molar ratio of 1:1 was sealed inside an evacuated quartz tube. The sealed tube was placed into a box furnace which was then heated to 220 °C and held for 12hrs.

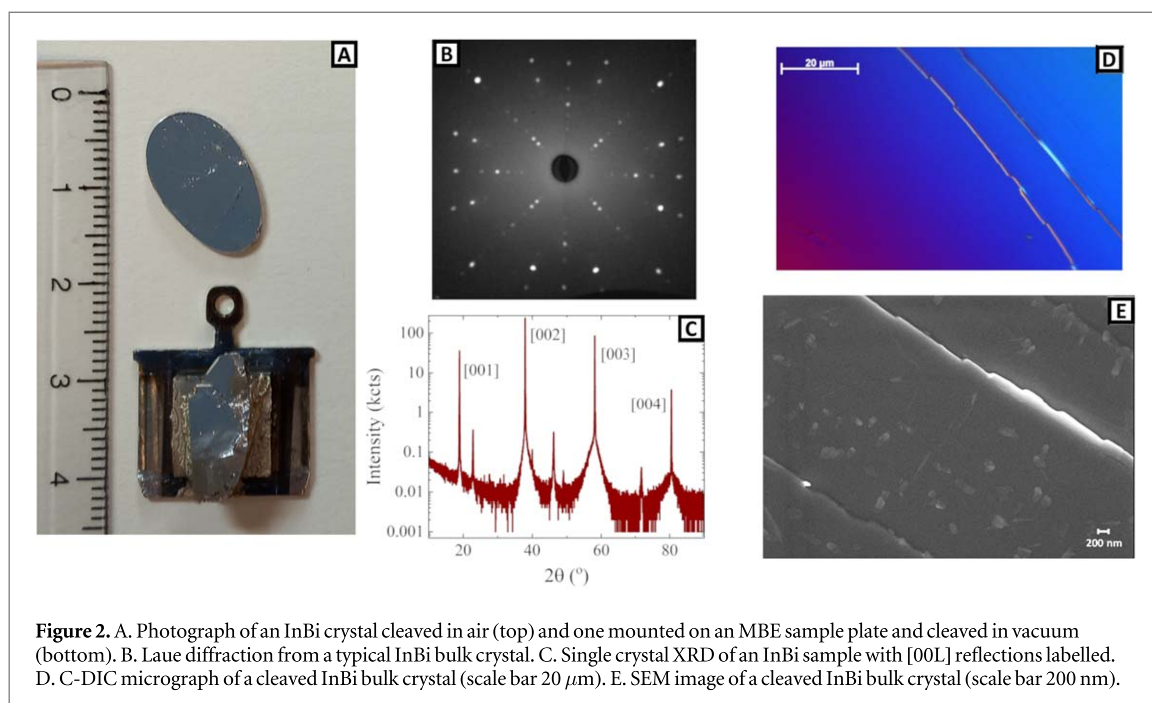

Figure 2. A. Photograph of an InBi crystal cleaved in air (top) and one mounted on an MBE sample plate and cleaved in vacuum (bottom). B. Laue diffraction from a typical InBi bulk crystal. C. Single crystal XRD of an InBi sample with [00L] reflections labelled. D. C-DIC micrograph of a cleaved InBi bulk crystal (scale bar 20 μm). E. SEM image of a cleaved InBi bulk crystal (scale bar 200 nm).

The furnace was then slowly cooled to room temperature at 2 °C per hour. Crystals could be cleaved with a razor blade both in ambient conditions and in UHV, the latter using a blade mounted on a wobble-stick in the sample storage chamber of the MBE system. For this procedure, samples were mounted to carrier plates using vacuum-compatible conductive epoxy glue (figure 2(A)).

Epitaxy studies were performed using shuttered effusion cells for Bi and In. All growth was performed with the InBi substrate crystals at 60°C, as measured by a thermocouple close to the sample position. For all experiments reported here, PSE was used, i.e. substrates were sequentially exposed to Bi or In fluxes [21], rather than conventional MBE with coincident fluxes. The background pressure was 2×10^{-8} Pa. The growth rate was estimated from the suppression of Sb XPS signal in previous heteroepitaxy work on InSb substrates [21] and was around 4 InBi Ml min^{-1}.

Bulk samples were analyzed using x-ray diffraction (XRD) and Laue diffraction, circular polarized differential interference contrast (C-DIC) microscopy, scanning electron microscopy (SEM) and atomic force microscopy (AFM). Epitaxial samples were additionally analyzed by RHEED, with patterns recorded before and during PSE growth using a 5 keV electron beam. X-ray photoelectron spectroscopy (XPS) was applied in an analysis chamber attached to the MBE system. Work functions of several cleaved InBi crystals were also measured by Kelvin probe, and their room temperature resistivity measured by four-point probe.

3. Results and discussion

Crystal boules of up to 10 mm diameter were grown. Examples are shown in figure 2(A). Sample cleaving in ambient air using a sharp blade usually produced mirror-like surfaces. Rough fracture features sometimes appeared, particularly when cleaving in vacuum where blade alignment is more difficult. Although in-vacuum cleaves did not always produce usable substrates, substantial mirror-like areas at least several mm across normally resulted allowing PSE and RHEED experiments.

The work function of several cleaved InBi(001) crystals was measured under flowing nitrogen to be 4.46 ± 0.08 eV. The variation between cleaves or samples was a few tens of meV. Liu, Zheng and Jiang [33] calculated work functions for the (110) cleave surfaces of 12 III-V compounds in the zincblende (zb) structure, including III-Bi compounds. They found that work function correlated with cohesive energy for all the materials, with zb-InBi the lowest among the 12 (2.71 eV/atom and 4.32 eV respectively). Even though InBi does not form a zincblende structure, its work function should be low among the III-V materials because of its lower cohesive energy. The experimental value for the tetragonal InBi(001) cleave surface found here is not far from that of the calculated zb-InBi(110) cleave surface.

The average value value of room temperature resistivity was 1.4 $\mu\Omega$ m, closely comparable to the value of low temperature resistivity multiplied by residual resistivity ratio as reported by Ekahana *et al* [20] which was taken as an indication of high crystal quality.

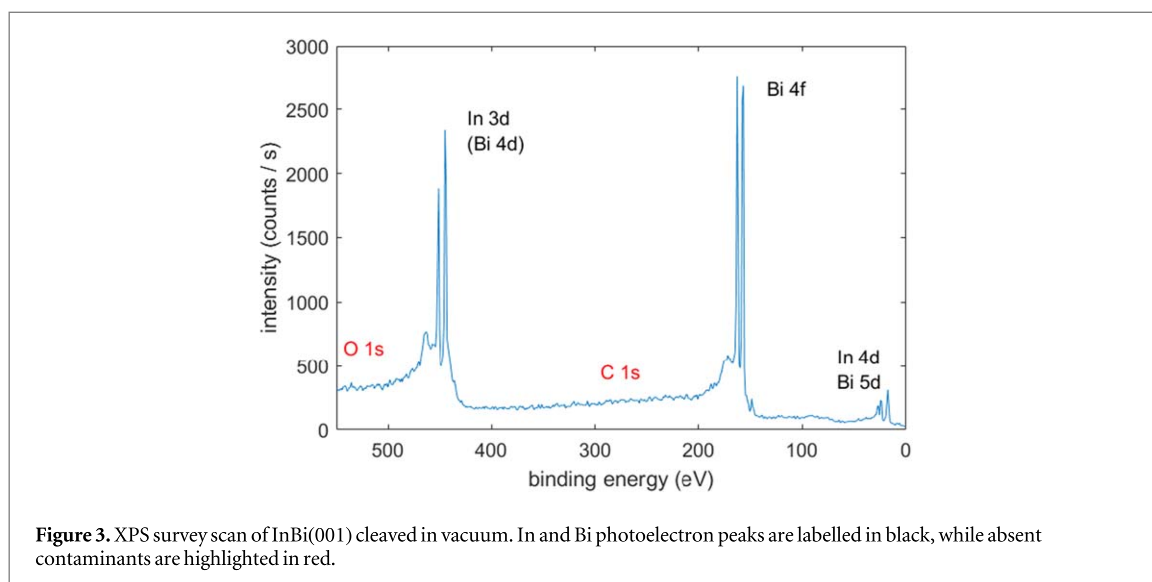

Figure 3. XPS survey scan of InBi(001) cleaved in vacuum. In and Bi photoelectron peaks are labelled in black, while absent contaminants are highlighted in red.

A Laue diffraction pattern from a cleaved crystal is shown in figure 2(B) and exhibits the expected fourfold symmetry, with intense diffraction spots on a low background. In in figure 2(C) we show XRD results from a large InBi crystal, with the source and detector symmetrically disposed about the cleaved surface normal. The expected (00*l*) reflections are observed ($l = 1–4$). Four additional peaks are seen at much lower intensity, representing impurity phases with probably less than 1% of the sample volume. The most likely candidates are unreacted In and Bi: 39° for In (110), and 22.8°, 46.2° and 71.8° for the (00*l*) family of Bi. Figure 2(D) shows a C-DIC micrograph from a cleaved surface. Large terraces are separated by fracture features. The 'optical' terrace width is typically tens of μm, although this can vary widely depending on the cleave quality. Higher resolution SEM is shown in figure 2(E), which reveals steps or step bunches separated by flat terraces several μm wide. However, contrast can be seen within a single terrace, with brighter patches up to about 200 nm across covering a few % of the terrace area.

A typical XPS survey scan from a InBi(001) surface prepared by cleaving in vacuum is shown in figure 3. Strong doublets for In 3d and Bi 4f dominate the spectrum. Quantification using approximate relative sensitivity factors is consistent with stoichiometric quantities of In and Bi, as expected. The In $3d_3$ and Bi $4f_5$ peaks can be fitted with single asymmetric peaks: there is no evidence for chemically shifted or surface shifted components at the energy resolution of the XPS system used (1.2 eV FWHM for Ag 3d). Contaminant peaks (O and C 1s) are absent. They do not appear after PSE experiments, but the In:Bi ratio is affected by PSE. This means that In and Bi layers, clusters or droplets are sticking to the InBi surface and affecting the measured stoichiometry. Further XPS results are shown in Supporting Information.

AFM topographs, along with line profiles, are shown in figure 4 for samples of cleaved InBi(001). The overall topography is very flat and only small-scale images are shown. These images were obtained in ambient conditions, which leads to some streaky noise in the images, and steps are somewhat rounded by tip convolution. Still, the vertical resolution is sufficient to reliably measure step heights between adjacent terraces. Panels A and D show what appears to be a single terrace, i.e. no long, straight steps or step bunches due to the cleave pass through the image. However, shallow pits with width tens of nm can be observed. A line profile through these reveals them to be approximately 0.24 nm deep. Panel B shows a step of full ML height (≈ 0.5 nm) running roughly vertically, but shallower pit / terrace features are visible on the upper and lower main terraces. Again, their depths are about half ML step height. Figure 4(C) shows a double-ML step running approximately vertically (height just under 1 nm). Pits of 1 ML and half-ML depth are again visible on the main terraces. This shows the ubiquity of half-ML height steps on cleaved InBi(001), demonstrating the necessity of terminating the surface with both atomic species (figure 1).

RHEED patterns during PSE of InBi on a typical cleaved InBi(001) substrate are illustrated in figure 5. After the initial cleave, strong surface diffraction and Kikuchi features are clear. The Kikuchi patterns are different in detail from standard III-V semiconductors with the zincblende structure. For example, in figure 5(A), left panel, the broad central vertical bright streak flanked by darker triangles is similar to that observed in a $\langle 110 \rangle$ azimuth for cubic III-Vs. However, the characteristic single dark triangle of the cubic III-V $\langle 100 \rangle$ azimuth does not appear for InBi $\langle 100 \rangle$. The in-plane lattice parameters derived from RHEED are $a = 4.94 \pm 0.06$ Å and $b = 5.03 \pm 0.06$ Å, which are identical within the error bar and consistent with previous determinations [20, 34]. Under all PSE conditions, only (1×1) periodicity was observed. On very limited regions of a few cleaved surfaces, one or two parallel streaks separated by a small fraction of the integer order spacing (typically one tenth to one

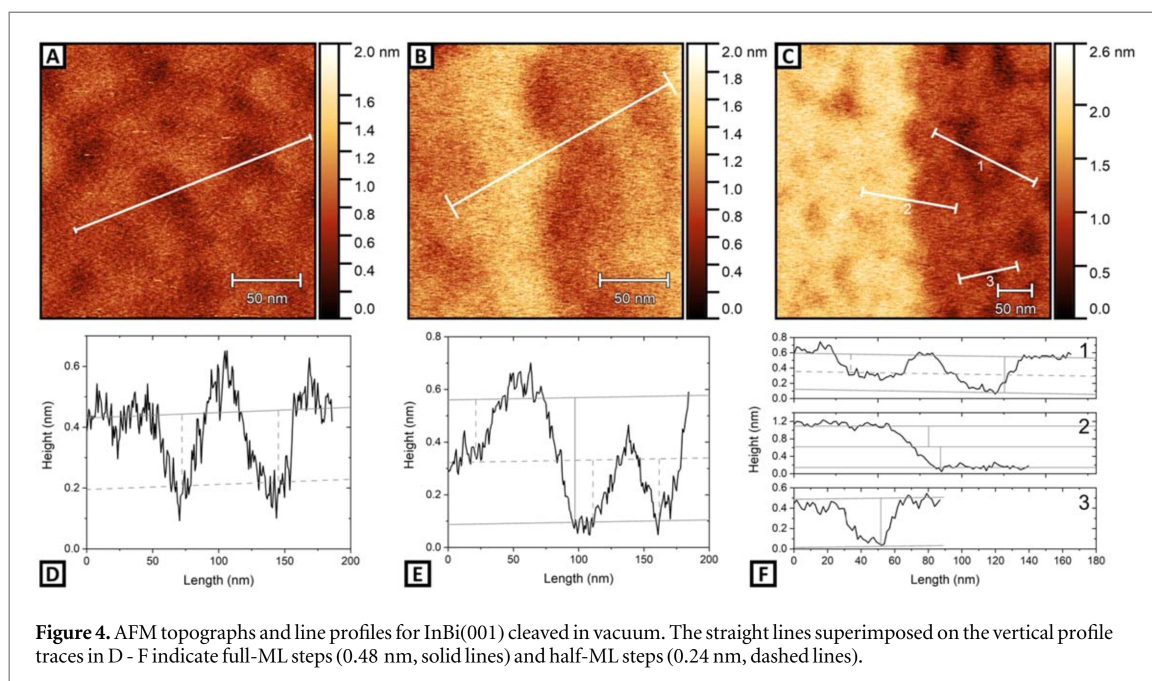

Figure 4. AFM topographs and line profiles for InBi(001) cleaved in vacuum. The straight lines superimposed on the vertical profile traces in D - F indicate full-ML steps (0.48 nm, solid lines) and half-ML steps (0.24 nm, dashed lines).

twentieth) were observed flanking the main streaks. An example is shown in Supporting Information. These small separations in reciprocal space correspond to long-range periodicities in real space. The most likely candidate is small patches of quasi-periodic step-terrace arrays from the cleave. However, no low-order fractional streaks were observed on any samples, confirming that the InBi(001) surface does not reconstruct. This is consistent with low energy electron diffraction (LEED) and STM results for InBi(001) on InAs(111) [27]. Figure 5(B) shows the RHEED patterns after a short exposure to the Bi flux. Most of the Kikuchi features are suppressed, presumably owing to the strong scattering from surface Bi atoms. The streaky pattern is replaced by an array of features which can be attributed to transmission diffraction. These are laterally extended, indicating some in-plane disorder. In-plane lattice spacings are indicated in red: 4.1 ± 0.1 Å and 2.8 ± 0.1 Å . The transmission diffraction allows the out-of-plane lattice spacing to be estimated, at around 6.1 Å. A second set of sharper features is superimposed on these transmission diffraction features. Their in-plane spacings are consistent with InBi(001), and their positioning is consistent with the original streaks (particularly obvious in the [110] and [100] azimuths). Therefore they can be attributed to exposed regions of the substrate. This RHEED pattern implies formation of crystalline Bi nano-clusters on the surface. A cubic Bi structure with $a = 3.18$ Å was previously reported [35, 36]. If the out-of-plane parameter were doubled and a very large in-plane strain of 12% were present, such a structure would be consistent with the observed RHEED pattern. Nano-scale Bi clusters have been observed to transition between rhombohedral and cubic structures at a critical size of 8.4 nm, and structural instability is reported below 6 nm [37, 38]. Such effects may account for the apparent high strain and in-plane disorder in the RHEED.

The subsequent indium flux planarizes the surface, as shown in figure 5(C), with the transmission diffraction features completely disappearing. A similar effect was previously observed for heteroepitaxy of InBi on InSb [21]. However, the pattern does not recover to the quality of the cleaved surface. In particular, the Kikuchi features are weakened significantly and the intensity of the surface diffraction features is reduced. Furthermore, faint powder diffraction rings are also visible, particularly in the [010] direction, which likely indicates polycrystalline (non-epitaxial) InBi grain formation.

The results of a further cycle of Bi (45 s) and In (45 s) deposition are shown in figures 5(D) and (E). Integer order surface diffraction features remain visible, with no significant changes in lattice parameter, but the continuous background intensity becomes even higher suggesting a more disordered structure. Ring-like intensity modulation implies a continued polycrystalline contribution to the diffraction. In the limited number of epitaxy experiments performed (since each requires a new bulk crystal cleave) it was not possible to find a PSE protocol which preserved streaky RHEED patterns beyond the first cycles of deposition. This suggests that homoepitaxy under these conditions is difficult, with surfaces rapidly degrading via 3D growth. The result is consistent with the degradation of RHEED patterns typically observed in heteroepitaxy of InBi on InSb(001) after several ML deposition [21] and with earlier studies on InBi heteroepitaxy by MBE [23]. Figure 6 shows an AFM topograph after PSE on a cleaved InBi(001) crystal together with three height profiles. Rather than step-terrace arrays, the sample topography is now dominated by clusters, confirming the 3D growth inferred from RHEED. Some have rectangular symmetry, such as the island beneath line profile 1, and clear terraces. These

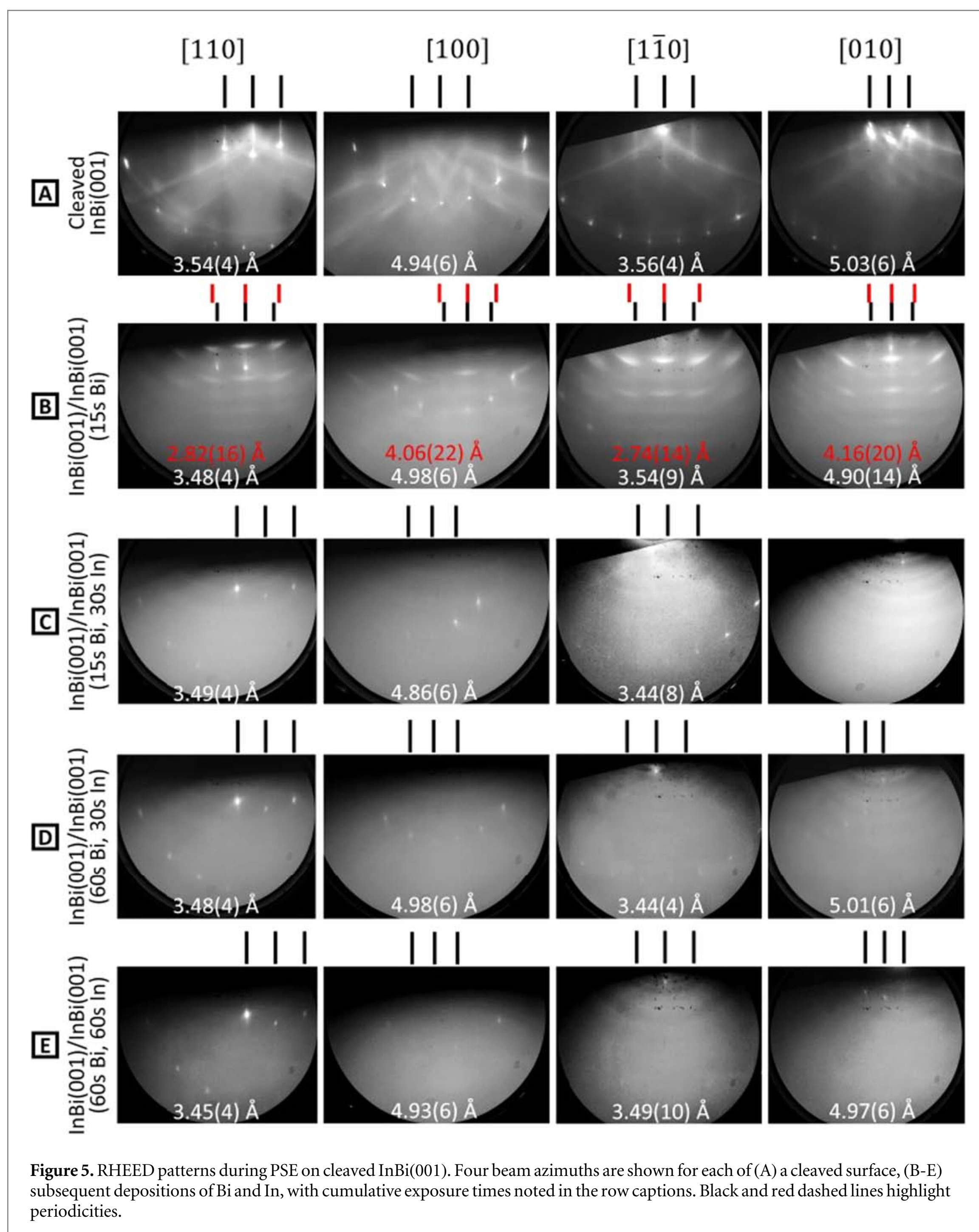

Figure 5. RHEED patterns during PSE on cleaved InBi(001). Four beam azimuths are shown for each of (A) a cleaved surface, (B-E) subsequent depositions of Bi and In, with cumulative exposure times noted in the row captions. Black and red dashed lines highlight periodicities.

appear to be epitaxial islands whose symmetry compatible with either In or InBi. In the case shown in figure 6, the height of the uppermost terrace is around 20 nm, around 40 InBi MLs. More common are rounded droplet-like clusters. Two examples are highlighted by profiles 2 and 3, showing typical heights of a few tens of nm and similar widths. It is not clear which types of cluster are associated with which element (or indeed if one type InBi). A very rough estimate from the AFM topographs suggests that around 1 ML of material is contained in the small clusters and another 1 ML in rectangular terraced islands. For the PSE durations employed, this leaves around 1 ML of material incorporated by 2D growth. It was not possible to clearly identify any half-ML steps between the underlying terraces, although imaging was more difficult in the presence of the 3D clusters. It is plausible that the incorporation of material via 2D growth is sufficient to relieve the two-species termination of the cleaved crystals but more detailed experiments (for example, with *in situ* STM) are needed to test this.

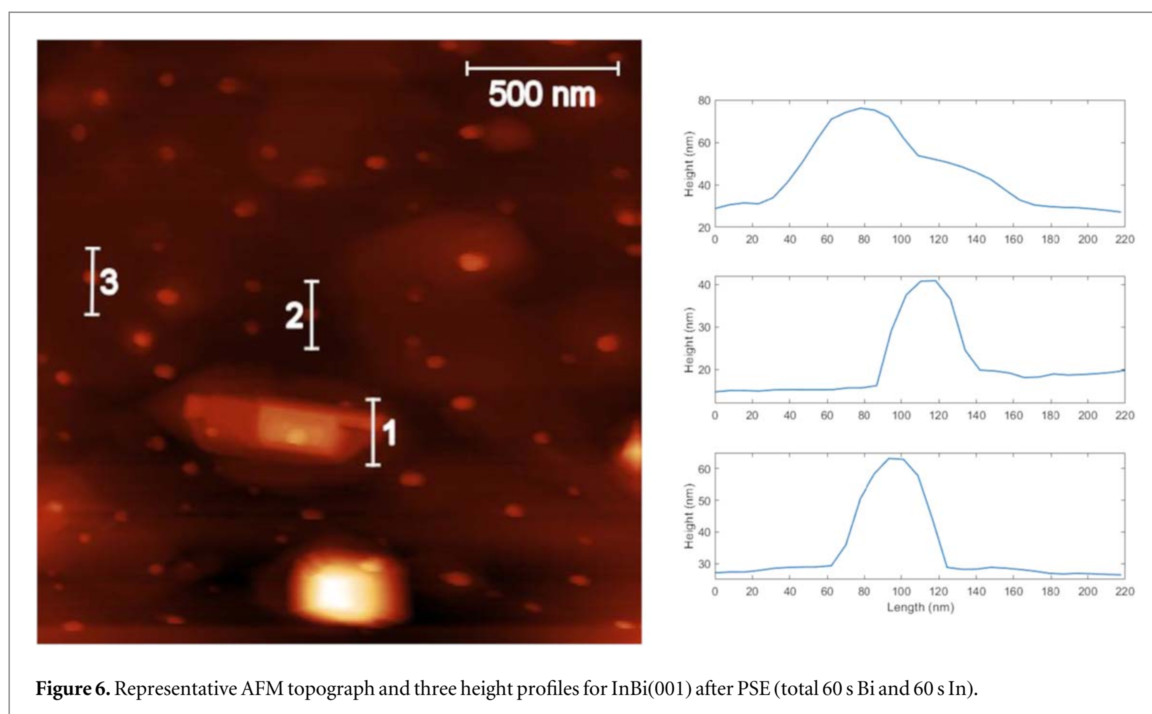

Figure 6. Representative AFM topograph and three height profiles for InBi(001) after PSE (total 60 s Bi and 60 s In).

4. Conclusions

High quality InBi bulk crystals have been grown by the modified Bridgman technique. They are readily cleaved on the [001] plane. The cleaved surfaces show termination with both In and Bi atomic planes, as evidenced by half-ML height atomic steps. This is similar to the termination observed by STM for InBi grown epitaxially on InAs [27] and unique among III-V polar bulk terminations. This result implies that heteroepitaxial growth of a III-V semiconductor on top of InBi(001) must account for the mixed termination, which may promote antiphase domains or other extended defects, as found in III-V / IV heteroepitaxy [39, 40] and other heteroepitaxial systems [41, 42]. As explored for heteroepitaxial InBi(001) on InAs(111)A, the surface termination of InBi affects the band structure observed in ARPES [27], and the present work shows that this should also be true for studies of cleaved InBi(001), hence possibly requiring reinterpretation of existing results [20].

Homoepitaxy of InBi on InBi(001) surfaces prepared in vacuum by cleaving was hampered by rapid formation of 3D nano-structures possibly comprising In or Bi and InBi. The difficulty of homoepitaxial growth of InBi is confirmed by these results, which must also translate to heteroepitaxial growth after the underlying substrate is completely covered [21, 23, 24]. It is not yet clear whether exposure to Bi or In fluxes can remove the half-ML height steps present after cleaving without also promoting cluster / droplet formation. Because the surface states depend strongly on the surface termination [27] this could be used to tailor the topological properties.

Acknowledgments

TJR was supported by the Doctoral Training Partnership (EPSRC, UK). Crystal growth was supported by EPSRC grant EP/T005963/1.

TB and JM acknowledge the support by the QM4ST project financed by the Ministry of Education of the Czech Republic grant no. CZ.02.01.01/00/22-008/0004572, co-funded by the European Regional Development Fund.

Data availability statement

The data that support the findings of this study are available upon reasonable request from the authors.

References

[1] Vergniory M G, Elcoro L, Felser C, Regnault N, Bernevig B A and Wang Z 2019 A complete catalogue of high-quality topological materials *Nature* **566** 480–5

[2] Bansil A, Lin H and Das T 2016 Colloquium: topological band theory *Rev. Mod. Phys.* **88** 021004

[3] Po H C, Vishwanath A and Watanabe H 2017 Complete theory of symmetry-based indicators of band topology *Nat. Commun.* **8**

[4] Armitage N P, Mele E J and Vishwanath A 2018 Weyl and Dirac semimetals in three-dimensional solids *Rev. Mod. Phys.* **90** 015001

[5] Hu J, Xu S-Y, Ni N and Mao Z 2019 *Annual Review of Materials Research* 49 ed D Clarke 207–52

[6] Fang C, Weng H, Dai X and Fang Z 2016 Topological nodal line semimetals *Chin. Phys.* B **25** 117106

[7] Vandenberghe W G and Fischetti M V 2017 Imperfect two-dimensional topological insulator field-effect transistors *Nat. Commun.* **8** 14184

[8] Collins J L *et al* 2018 Electric-field-tuned topological phase transition in ultrathin Na3Bi *Nature* **564** 390–4

[9] Xu N, Xu Y and Zhu J 2017 Topological insulators for thermoelectrics *NPJ Quantum Materials* **2** 51

[10] Ivanov Y V, Burkov A T and Pshenay-Severin D A 2018 Thermoelectric properties of topological insulators *Phys. Status Solidi* B **255** 1800020

[11] Elhoussieny I G, Rehaag T J and Bell G R 2023 Bulk and surface electrical properties of bisb on flat and ion-beam nano-patterned InP substrates *Phys. Status Solidi* B **260** 2300337

[12] Brahlek M, Lapano J and Lee J S 2020 Topological materials by molecular beam epitaxy *J. Appl. Phys.* **128** 210902

[13] Yang T, Yang Y, Wang X, Zhang G and Cheng Z 2023 Topological thermoelectrics: new opportunities and challenges *Materials Today Chemistry* **30** 101488

[14] Yang M, Zhou H and Wang J 2022 Topological insulators photodetectors: preparation, advances and application challenges *Materials Today Communications* **33** 104190

[15] Lin H, Wray L A, Xia Y, Xu S, Jia S, Cava R J, Bansil A and Hasan M Z 2010 Half-Heusler ternary compounds as new multifunctional experimental platforms for topological quantum phenomena *Nat. Mater.* **9** 546–9

[16] Kong D *et al* 2011 Rapid surface oxidation as a source of surface degradation factor for Bi2Se3 *ACS Nano* **5** 4698–703

[17] Chang J, Jadaun P, Register L F, Banerjee S K and Sahu B 2011 Dielectric capping effects on binary and ternary topological insulator surface states *Phys. Rev.* B **84** 155105

[18] Bansal N *et al* 2011 Epitaxial growth of topological insulator Bi2Se3 film on Si(111) with atomically sharp interface *Thin Solid Films* **520** 224–9

[19] Pan H, Wu M, Liu Y and Yang S A 2015 Electric control of topological phase transitions in Dirac semimetal thin films *Sci. Rep.* **5** 14639

[20] Ekahana S A *et al* 2017 Observation of nodal line in non-symmorphic topological semimetal InBi *New J. Phys.* **19** 065007

[21] Rehaag T J and Bell G R 2024 Heteroepitaxial growth of InBi(001) *Molecules* **29** 2825

[22] Manasijevic I, Balanovic L, Grguric T H, Minic D and Gorgievski M 2019 Study of microstructure and thermal properties of the low-melting Bi-In eutectic alloys *J. Therm. Anal. Calorim.* **136** 643–9

[23] Keen B, Makin R, Stampe P A, Kennedy R J, Sallis S, Piper L J, McCombe B and Durbin S M 2014 Growth parameters for thin film inbi grown by molecular beam epitaxy *J. Electron. Mater.* **43** 914–20

[24] Dang P, Rouvimov S, Xing H G and Jena D 2019 Magnetotransport and superconductivity in InBi films grown on Si(111) by molecular beam epitaxy *J. Appl. Phys.* **126** 103901

[25] Hsu C-H, Huang Z-Q, Lin C-Y, Macam G M, Huang Y-Z, Lin D-S, Chiang T C, Lin H, Chuang F-C and Huang L 2018 Growth of a predicted two-dimensional topological insulator based on InBi-Si(111)-7 x 7 *Phys. Rev.* B **98** 121404

[26] Binnie W 1956 The structural crystallography of indium bismuthide *Acta. Cryst.* **9** 686–7

[27] Nicolaï L *et al* 2024 Topological material in the III–V family: heteroepitaxial InBi on InAs *Phys. Rev. Res.* **6** 043116

[28] Krzyzewski T, Joyce P, Bell G and Jones T 2002 Wetting layer evolution in InAs/GaAs(001) heteroepitaxy: effects of surface reconstruction and strain *Surf. Sci.* **517** 8–16

[29] Bell G, Belk J, McConville C and Jones T 1999 Species intermixing and phase transitions on the reconstructed (001) surfaces of GaAs and InAs *Phys. Rev.* B **59** 2947–55

[30] Ivanov M, Gomez D, Hannikainen K, Niu Y R and Pereiro J 2022 Unified method for measuring entropy differences between coexisting surface phases using low energy electron microscopy *Phys. Rev. Res.* **4** 033163

[31] Zheng C X, Hannikainen K, Niu Y R, Tersoff J, Gomez D, Pereiro J and Jesson D E 2019 Mapping the surface phase diagram of GaAs (001) using droplet epitaxy *Phys. Rev. Mater.* **3** 124603

[32] Dutta P 2011 *Comprehensive Semiconductor Science and Technology* ed P Bhattacharya, R Fornari and H Kamimura (Elsevier) 36–80

[33] Liu W, Zheng W T and Jiang Q 2007 First-principles study of the surface energy and work function of III-V semiconductor compounds *Phys. Rev.* B **75** 235322

[34] Nikolic P, Todorovic D, Vasiljevic-Radovic D, Vujatovic S, Radulovic K, Duric S, Blagojevic V, Urosevic D, Mihajlovic P and Elazar J 2000 Photoacoustic investigation of anisotropic thermal and transport properties of single crystal InBi *11th International Conference on Photoacoustic and Photothermal PhenomenaAnalytical Sciences 2001* 17 *(Kyoto, Japan, Jun 06-09 2000)* S148–50

[35] Jaggi R 1964 Struktur und eigenschaften der hochdruck-modifikation bi II *Helv. Phys. Acta* **37** 618–9

[36] Sadowski J, Kaleta A, Kryvyi S, Janaszko D, Kurowska B, Bilska M, Wojciechowski T, Domagala J Z, Sanchez A M and Kret S 2022 Bi incorporation and segregation in the MBE-grown GaAs-(Ga,Al)As-Ga(As,Bi) core–shell nanowires *Sci. Rep.* **12** 6007

[37] Oshima Y, Takayanagi K and Hirayama H 1997 Structural anomaly of fine bismuth particles observed by ultra high-vacuum TEM *Zeitschrift für Physik D Atoms,Molecules and Clusters* **40** 534–8

[38] Yokozeki A and Stein G D 1978 A metal cluster generator for gas-phase electron diffraction and its application to bismuth, lead, and indium: Variation in microcrystal structure with size *J. Appl. Phys.* **49** 2224–32

[39] Kvam E P 1994 Interactions of dislocations and antiphase (inversion) domain boundaries in III-V/IV heteroepitaxy *J. Electron. Mater.* **23** 1021–6

[40] Koh S, Kondo T, Ishiwada T, Iwamoto C, Ichinose H, Yaguchi H, Usami T, Shiraki Y and Ito R 1998 Sublattice reversal in GaAs/Si/GaAs (100) heterostructures by molecular beam epitaxy *Japan. J. Appl. Phys.* 2 **37** L1493–6

[41] Nedelkoski Z, Sanchez A M, Ghasemi A, Hamaya K, Evans R F L, Bell G R, Hirohata A and Lazarov V K 2016 The antiphase boundary in half-metallic Heusler alloy Co2Fe(Al,Si): atomic structure, spin polarization reversal, and domain wall effects *Appl. Phys. Lett.* **109** 222405

[42] Zweck U, Neibecker P, Mühlbauer S, Zhang Q, Chiu P-Y and Leitner M 2022 Magnetization reversal induced by antiphase domain boundaries in Ni2MnZ Heusler compounds *Phys. Rev.* B **106** 224106